Open Access Full Text Article

ORIGINAL RESEARCH

FPR1, as a Potential Biomarker of Diagnosis and Infliximab Therapy Responses for Crohn's Disease, is Related to Disease Activity, Inflammation and Macrophage Polarization

Chenglin Ye[1],*, Sizhe Zhu [2],*, Jingping Yuan[1], Xiuxue Yuan[3]

[1]Department of Pathology, Renmin Hospital of Wuhan University, Wuhan, Hubei, People's Republic of China; [2]Department of Otolaryngology-Head and Neck Surgery, Tongji Hospital, Tongji Medical College, Huazhong University of Sciences and Technology, Wuhan, Hubei, People's Republic of China; [3]Medical College of Wuhan University of Science and Technology, Wuhan, Hubei, People's Republic of China

*These authors contributed equally to this work

Correspondence: Jingping Yuan; Xiuxue Yuan, Email yuanjingping@whu.edu.cn; exiuwust@gmail.com

Purpose: Crohn's disease (CD) represents a multifaceted inflammatory gastrointestinal condition, with a profound significance placed on unraveling its molecular pathways to enhance both diagnostic capabilities and therapeutic interventions. This study focused on identifying a robust macrophage-related signatures (MacroSig) for diagnosing CD, emphasizing the role of FPR1 in macrophage polarization and its implications in CD.

Patients and Methods: Expression profiles from intestinal biopsies and macrophages of 1804 CD patients were retrieved from the Gene Expression Omnibus (GEO). Utilizing CIBERSORTx, differential expression analysis, and weighted correlation network analysis to to identify macrophage-related genes (MRGs). By unsupervised clustering, distinct clusters of CD were identified. Potential biomarkers were identified via using four machine learning algorithms, leading to the establishment of MacroSig which combines insights from 12 machine learning algorithms. Furthermore, the expression of FPR1 was verified in intestinal biopsies of CD patients and two murine experimental colitis models. Finally, we further explored the role of FPR1 in macrophage polarization through single-cell analysis as well as through the study of RAW264.7 cells and peritoneal macrophages.

Results: Two distinct clusters with differential levels of macrophage infiltration and inflammation were identified. The MacroSig, which included FPR1 and LILRB2, exhibited high diagnostic accuracy and outperformed existing biomarkers and signatures. Clinical analysis demonstrated a strong correlation of FPR1 with disease activity, endoscopic inflammation status, and response to infliximab treatment. The expression levels of FPR1 were validated in our CD cohort by immunohistochemistry and confirmed in two colitis mouse models. Single-cell analysis indicated that FPR1 is predominantly expressed in macrophages and monocytes. In vitro studies demonstrated that FPR1 was upregulated in M1 macrophages, and its activation promoted M1 polarization.

Conclusion: We developed a promising diagnostic signature for CD, and targeting FPR1 to modulate macrophage polarization may represent a novel therapeutic strategy.

Keywords: Crohn's disease, macrophage, diagnostic signature, FPR1, machine learning

Introduction

Crohn's disease (CD) is a subtype of inflammatory bowel disease (IBD) that affects the gastrointestinal tract.[1] The disease is characterized by periods of remission and relapse, with symptoms ranging from abdominal pain and diarrhea to severe complications such as fistulas and intestinal obstruction.[2] Since the 20th century, the global incidence of CD has increased markedly, particularly in emerging industrialized nations within Asia, Africa, and South America.[3] This rise is attributed to changes in lifestyle, dietary habits, and increased exposure to environmental risk factors in these regions.[4] The pathogenesis of CD involves multiple factors, including genetic predisposition, environmental influences, and immune system dysregulation.[5]

Dysfunction and hyperactivity in the immune response are key factors that contribute to uncontrolled inflammation, a defining feature of CD.[6] Consequently, addressing these factors is crucial in the treatment of CD.

Macrophages play a pivotal role in maintaining intestinal immune homeostasis.[7,8] The transition of macrophages from protectors to aggressors, under the influence of environmental and genetic determinants, represents a crucial element of CD pathogenesis.[8] Macrophages present heterogeneity and are known for two main phenotypes: the pro-inflammatory M1 and the anti-inflammatory M2. M1 macrophages, stimulated by bacterial lipopolysaccharide (LPS), exacerbate inflammation through the production of cytokines like tumor necrosis factor alpha (TNF-α), interleukin (IL)-1β, IL-6, and IL-23. On the contrary, M2 macrophages, when activated by IL-4, boost tissue repair and resolution of inflammation by releasing anti-inflammatory cytokines like arginase 1 and IL-10.[9–12] In CD, the balance between M1 and M2 macrophages is disrupted,[13] and exploring the mechanism of regulating macrophage polarization in CD is crucial, as it may provide the groundwork for developing novel therapeutic targets and strategies.

In this study, we identified macrophage-related genes (MRGs) using expression profiles of intestinal macrophages isolated from CD patients and further constructed a macrophage-related signature (MacroSig) for CD diagnosis by integrating 12 machine learning algorithms. Subsequently, we identified formyl peptide receptor 1 (FPR1) as a novel potential biomarker for CD diagnosis and predicting the outcome of anti-TNF therapy in CD patients. We also found that FPR1 was upregulated in CD and validated it in our CD cohort as well as in two colitis mouse models. Furthermore, single-cell RNA sequencing (scRNA-seq) data revealed that FPR1 was highly expressed in monocytes and macrophages, and we investigated the role of FPR1 in macrophage polarization in peritoneal macrophages (PMs) and RAW264.7 cells.

Materials and Methods
Data Collection
The gene expression datasets used in this work were retrieved from the Gene Expression Omnibus (GEO; https://www.ncbi.nlm.nih.gov/geo/) and included the GSE93624, GSE57945, GSE123141, GSE179285, GSE126124, GSE16879, GSE3365, GSE193677, GSE186582 and GSE36537. The detailed information of the CD datasets is presented in Supplementary Table S1. The expression profile of intestinal macrophages in CD patients was obtained from the GSE123141.

Differentially Expressed Genes and Weighted Correlation Network Analysis (WGCNA)
Differentially expressed gene analysis was performed by limma R package.[14] The genes with an adjusted P value <0.05 and a |log2(fold change)| >0 were identified as differentially expressed genes (DEGs). WGCNA was used to identify the related modules via the SangerBox online tool.[15] The minimum number of module genes was set to 30, the parameter deep slip was set to 4, and the mergeCutHeight was set to 0.25. The hierarchical clustering dendrogram summarizes the gene modules with different colors.[16]

Unsupervised Clustering and Immune Infiltration Analysis
A consensus clustering algorithm was performed using the SangerBox online tool,[15] and the process was repeated 1000 times to ensure the stability of the clustering. To evaluate immune cell infiltration, the CIBERSORTx (https://cibersortx.stanford.edu) algorithm was applied.[17] The Wilcoxon test was used to compare immune cell infiltration between different groups.

Screening Biomarkers and Construction of Diagnostic Signature Based on Machine Learning
Four machine learning methods, namely, least absolute shrinkage and selection operator (LASSO) regression, support vector machine recursive feature elimination (SVM-RFE), eXtreme Gradient Boosting (XGBoost), and random forest (RF), were applied to screen MRGs in CD. Using the "glmnt" R package, LASSO regression was used to determine candidates through tenfold cross-validation.[18] The "e1071" package enabled SVM-RFE analysis, where the gene set with maximum tenfold cross-validation accuracy was chosen.[19] The "XGBoost" package highlighted the top 20 genes.[20] The RF method identified

MRGs with the highest 20 Gini coefficients.[21] The intersecting MRGs from these techniques were designated as the potential biomarkers of CD.

To construct a diagnostic model with high accuracy and stability, we integrated 12 machine learning algorithms and 113 algorithm combinations.[22] We employed a comprehensive set of algorithms, including RF, LASSO, Ridge, elastic network (Enet), Stepglm, SVM, glmBoost, Linear Discriminant Analysis (LDA), Gradient Boosting Machine (GBM), XGBoost, and NaiveBayes. The model development process involved the following steps: (a) The expression profiles of the hub MRGs were found from the previous step; (b) 113 algorithm combinations were performed on the hub MRGs, developing diagnostic models using 10-fold cross-validation within the GSE93624 dataset; (c) All models were validated across three datasets, GSE57945, GSE16879, GSE179285 and GSE126124; and (d) the area under the curve (AUC) was calculated for each model across validation datasets, with the highest mean AUC indicating the potential model.

Functional Enrichment Analysis and Single-Cell Analysis

The clusterProfiler and GOplot R packages were used for Gene Ontology (GO) and Kyoto Encyclopedia of Genes and Genomes (KEGG) pathway analysis, respectively.[23,24] Gene set variation analysis (GSVA) was performed with the GSVA R package.[25] The gene sets used for GSVA were downloaded from the Molecular Signatures Database (MSigDB). Single-cell analysis was performed on the CD dataset titled "PREDICT 2021 paper: CD" via the Single-cell Portal (https://singlecell.broadinstitute.org/single_cell). The "PREDICT 2021 paper: CD" included 201,883 single-cell transcriptomes obtained from 27 volunteers.

Induction of Experimental Colitis in Mice

Thirty specific pathogen-free female C57BL/6J mice (8–10 weeks old, weighing 20~22 g) were purchased from Beijing Vital River Laboratory Animal Technology Co., Ltd., and were randomly assigned to four groups. For dextran sulfate sodium salt (DSS)-induced colitis, 10 mice were administered 2.5% DSS (MP Biomedicals, M.W. 36,000–50,000 kDa) in drinking water for 10 days, while five control mice received drinking water without DSS. All mice were euthanized on the 10th day, and the colons were collected for further testing. 2,4,6-Trinitro-benzenesulfonic acid (TNBS) was used to induce colitis in mice as previously described.[26] Briefly, TNBS pre-sensitization solution was prepared by mixing 4 volumes of an acetone/olive oil solution (4:1) with 1 volume of 5% TNBS. TNBS solution was prepared by mixing 1 volume of 5% TNBS solution with 1 volume of absolute ethanol. The mice were treated with TNBS pre-sensitization solution on the shaved skin. One week later, the mice were fasted overnight and then intrarectally administered with TNBS solution. After that, the mice were placed in a head-down position to avoid expulsion of the fluid for a few minutes. All mice were euthanized on the 4th day, and the colons were collected for further testing.

Cell Culture

PMs were isolated from C57BL/6J mice using a previously described protocol.[27] RAW264.7 cells were purchased from Warner Bio Co., Ltd. (Wuhan, China). RAW264.7 cells and PMs were cultured in complete DMEM supplemented with 10% (v/v) fetal bovine serum and 1% penicillin/streptomycin (100 U/mL) at 37°C with 5% CO_2. For M1 macrophage polarization, the macrophages were incubated with LPS (L2880, Sigma) and INF-γ (MedChemExpress) for 24 hours. To explore the function of FPR1, macrophages were incubated with N-formyl-Met-Leu-Phe (fMLP; MedChemExpress), a selective FPR1 agonist, for 16 hours.

Human Sample Collection and Immunohistochemistry (IHC) Analysis

Formalin-fixed, paraffin-embedded (FFPE) tissue samples were collected from 20 CD patients and 10 healthy patients for IHC analysis at the Renmin Hospital of Wuhan University from 2022 to 2023. Immunohistochemical staining was performed using the standard EnVision complex method.[28] The primary antibody used was FPR1 (Signalway Antibody LLC). Two pathologists who were blinded to the clinical details independently conducted the examinations.

RNA Extraction and Quantitative PCR

Total RNA was extracted from fresh colon samples from mice utilizing TRIzol (Invitrogen Life Technologies). cDNA was synthesized from total RNA using the HiScript II 1st Strand cDNA Synthesis Kit (Vazyme). Quantitative PCR was performed with Taq Pro Universal SYBR qPCR Master Mix (Vazyme). The sequences of primers used for PCR in this study are provided in Supplementary Table S2.

Flow Cytometry Analysis

Cells were harvested and washed twice with ice-cold phosphate-buffered saline (PBS). They were then incubated with FITC anti-mouse CD86 antibody (Abcam, ab234237) on ice in the dark for 20 minutes, followed by a wash with FACS buffer (2% BSA in PBS). Analysis was performed using an LSR Fortessa flow cytometer (BD Biosciences, Franklin Lakes, NJ, USA) equipped with FACSDiva software. Data analysis was further extended using FlowJo software.

Statistical Analysis

All the statistical and bioinformatics analyses in this study were conducted with R (version 4.2.3). The analyses included the Wilcoxon rank sum test and *T*-test. The statistical correlations were assessed using either Spearman's or Pearson's tests. A p value of <0.05 was considered to indicate statistical significance.

Results

## Identification and Functional Enrichment Analysis of MRGs

The workflow of this work is presented in Figure 1. The CIBERSORTx algorithm was used to estimate the infiltration level of macrophages in intestinal samples from CD patients (GSE93624). Figure 2A–C shows that CD patients had higher infiltration levels of M0 and M1 macrophages, whereas the control group had higher infiltration levels of M2 macrophages. Differentially expressed gene analysis was performed on the GSE93624 and the intestinal macrophage expression profiles of CD patients and healthy controls were obtained from the GSE123141 (Figure 2D and E). Furthermore, we applied WGCNA to screen the gene modules associated with M0/1/2 macrophage infiltration. The soft threshold β was set to 5 to construct a scale-free network, whereas the scale R2 = 0.85 (Supplementary Figure S1A–C). As shown in Figure 2F, the black module was positively correlated with the infiltration of M0 macrophages (module trait correlation = 0.37) and M1 macrophages (module trait correlation = 0.65), whereas the blue module was positively correlated with the infiltration of M2 macrophages (module trait correlation = 0.26). The intersection of the black module, blue module, differentially expressed genes (DEGs) in GSE93624, and GSE123141 was defined as the MRG. A total of 85 MRGs were obtained for further analysis, and heatmaps of the MRGs in GSE93624 and GSE123141 are presented in Figure 2G and I.

To explore the biological function of the MRGs, we conducted GO and KEGG enrichment analyses. As shown in Figure 3A, MRGs were enriched in biological processes, including cytokine-mediated signaling pathways and cellular responses to stimuli. The top three enriched terms for molecular function and cellular component were receptor activity, cytokine receptor binding, cytokine activity and tertiary granule, early endosome, and vesicle lumen, respectively (Figure 3B and C). KEGG analysis revealed that the MRGs were primarily related to the NOD-like receptor signaling pathway, cytokine–cytokine receptor interaction, and influenza A (Figure 3D).

Unsupervised Clustering of MRGs

Furthermore, an unsupervised consensus clustering analysis was performed based on the expression profiles of the MRGs. As shown in Figure 4A and Supplementary Figure S2A–D, the maximum consistency was found at k = 2 in the consensus matrix plot. Therefore, k = 2 had the best clustering effectiveness for identifying two distinct clusters. Principal component analysis (PCA) revealed significant differences in the expression profiles of the MRGs in GSE93624 (Figure 4B). GSVA enrichment scores were calculated to explore signaling pathway activation in each cluster. Cluster 2 was significantly enriched in inflammation-related biological processes, including the IL6/JAK/STAT3 signaling pathway, inflammatory response, and interferon α/γ response (Figure 4C). CIBERSORTx analyses demonstrated that cluster 2 was characterized by high M0 and M1 macrophage infiltration (Figure 4D and E). However, cluster 1 had relatively high infiltration levels of
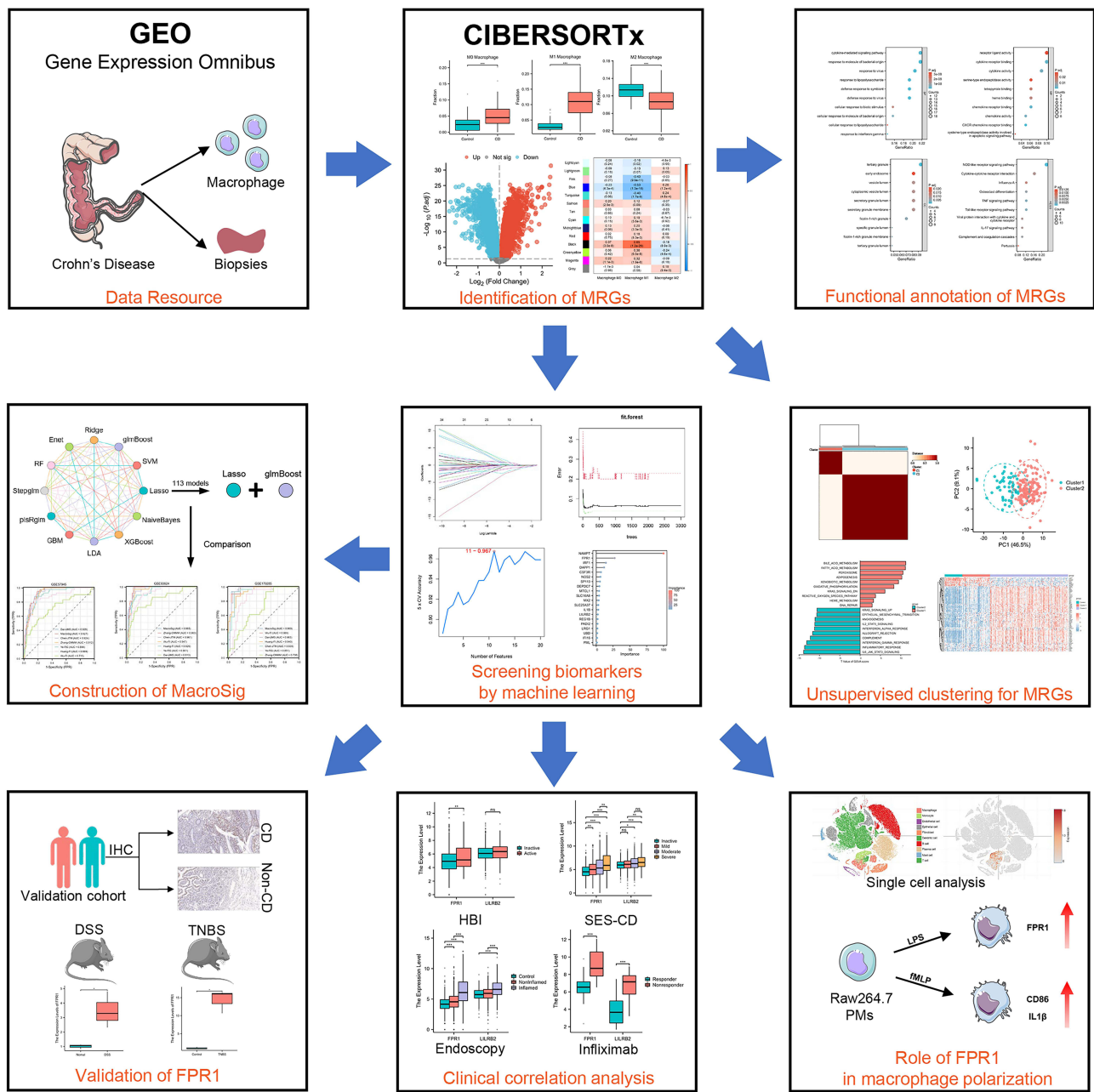
Figure 1 The workflow of this study. The figure was partly generated using Servier Medical Art, provided by Servier, licensed under a Creative Commons Attribution 3.0 unported license.

M2 macrophages (Figure 4F). A heatmap of MRGs in the control, cluster 1, and cluster 2 groups is presented in Figure 4G. The unsupervised consensus clustering analyses were validated in GSE57945. As shown in Supplementary Figure S3A–F, two clusters achieved the best clustering efficacy. Furthermore, cluster 1 and cluster 2 in GSE57945 had similar characteristics of macrophage infiltration. Cluster2 had higher infiltration levels of M0 and M1 macrophages, whereas the infiltration level of M2 macrophages was higher in cluster 1 (Supplementary Figure S3G–I). Taken together, the above results indicate that patients in cluster 2 may have relative higher inflammatory levels.

Screening Potential Biomarkers Based on Machine Learning

Eighty-five MRGs were used to screen potential biomarkers via machine learning. Twenty-six genes with clinical manifestations were selected using LASSO regression (Figure 5A and B). As shown in Figure 5C, the SVM-RFE
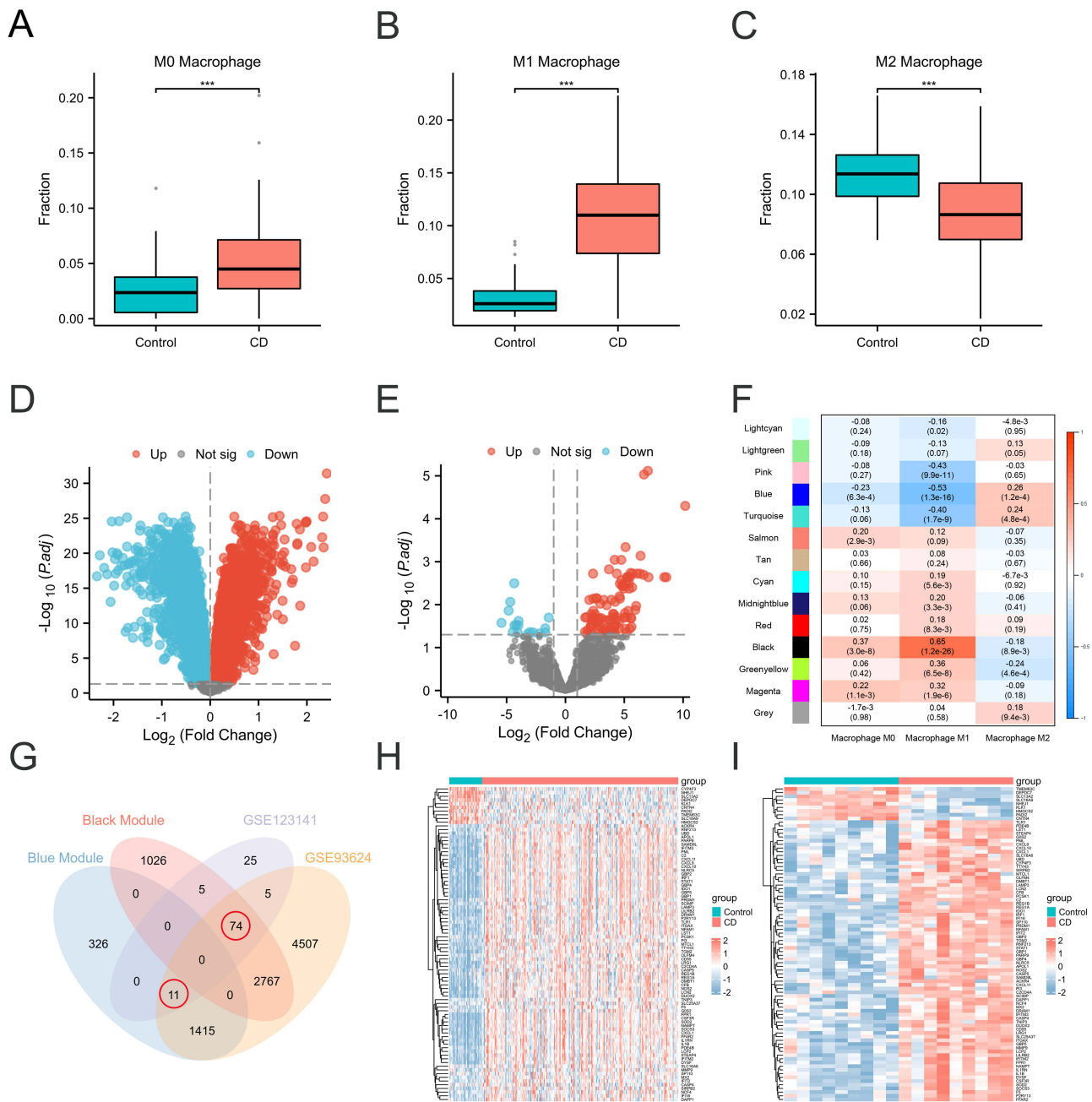
Figure 2 Identification of MRGs in CD. (**A–C**) The infiltration levels of M0, M1, and M2 macrophages in the control and CD groups. (**D–E**) Volcano plot of DEGs between the control and CD cohorts in the GSE93624 and GSE123141, respectively. (**F**) WGCNA module trait relationships in M0, M1, and M2 macrophages, which contained the corresponding correlation and p value. Each colored row on the left represents a gene module. (**G**) Intersection of DEGs; black and blue modules. (**H–I**) The heatmaps of MRGs in GSE93624 and GSE123141, respectively. (***p < 0.001).

algorithm identified 11 genes with maximum classification accuracy (0.967) by 5 cross-validations. The average rank of 11 genes is presented in Figure 5D. The top 20 important genes according to "Mean Decrease Gini" coefficient were screened via the RF algorithm (Figure 5E and F). The top 20 important genes according to the XGBoost algorithm are shown in Figure 5G. The outputs of the four machine learning algorithms were combined to obtain two potential biomarkers, namely, FPR1 and leukocyte immunoglobulin like receptor b2 (LILRB2) (Figure 5H).
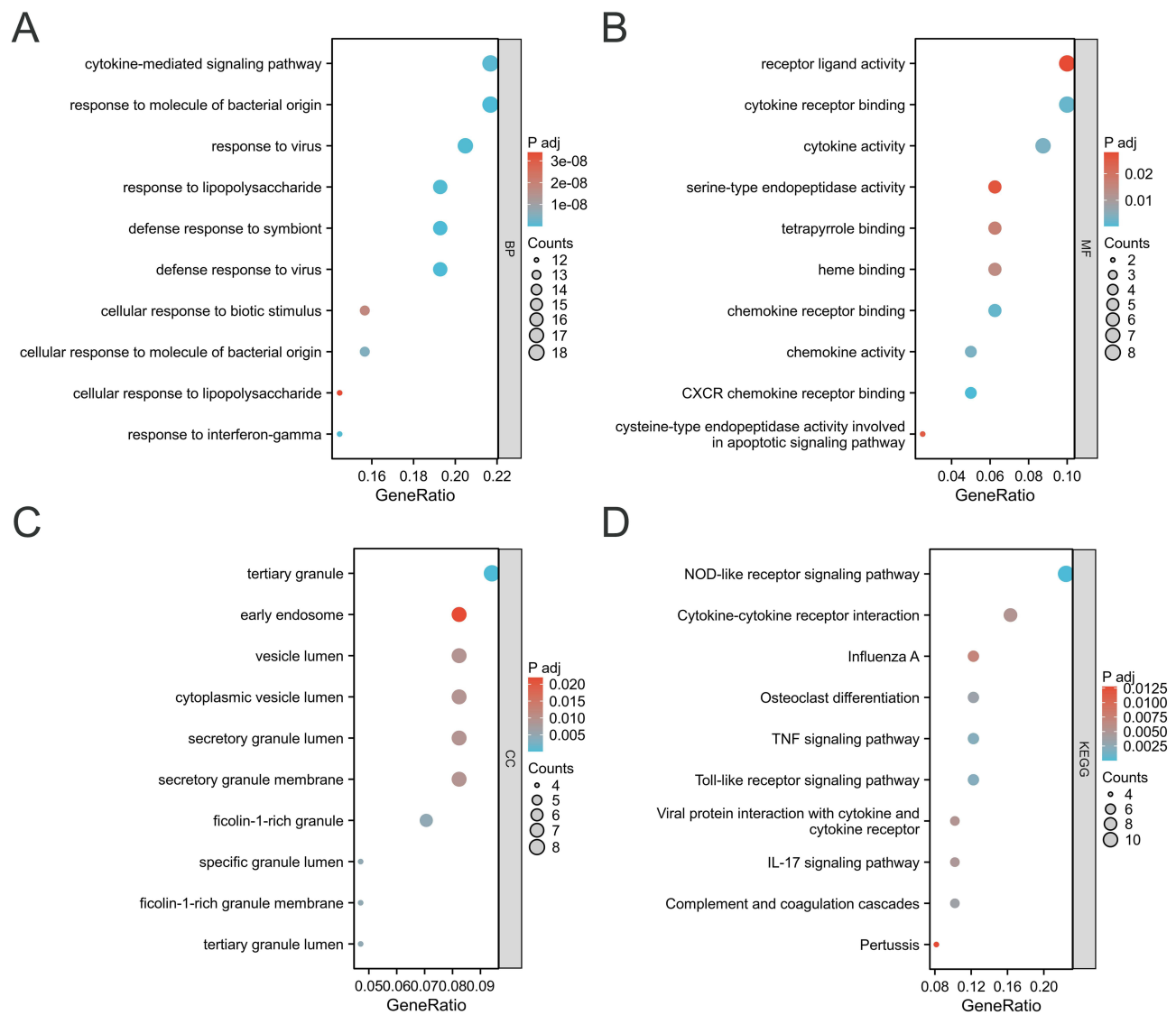
Figure 3 Functional annotation of MRGs. (**A**) Biological process. (**B**) Molecular function. (**C**) Cellular component. (**D**) KEGG pathway enrichment analysis.

Integrative Construction of a Diagnostic Signature

Based on the expression profiles of FPR1 and LILRB2, a machine learning-based integrative procedure was used to develop MacroSig. In training dataset GSE93624, 113 kinds of models were constructed via combining 12 machine learning algorithms and 10-fold cross-validation. The area under the curve (AUC) of each model was further calculated across the training dataset and all validation datasets, including GSE57945, GSE179285, GSE16879, and GSE126124 (Figure 6A and Supplementary Table S3). Notably, the combination of LASSO and glmBoost, which had the highest average AUC (0.952), was considered the optimal model.

Recently, with developments in next-generation sequencing and big-data technologies, a considerable number of diagnostic biomarkers and gene expression signatures have been developed based on machine learning.[29] To comprehensively compare the performance of MacroSig with that of other signatures and biomarkers, we systematically retrieved published signatures and biomarkers from CD studies. Overall, 6 signatures and biomarkers were evaluated (Supplementary Table S4).[30–35] Furthermore, the AUC of MacroSig was compared with that of other signatures and biomarkers. MacroSig ranked first in GSE93624, GSE179285, GSE16879, and GSE126124 and second in GSE57945 (Figure 6B–F). MacroSig displayed accuracy distinctively superior to that of the other signatures and biomarkers in almost all the datasets. We noticed that some signatures were detected in a few datasets but were weak in other external
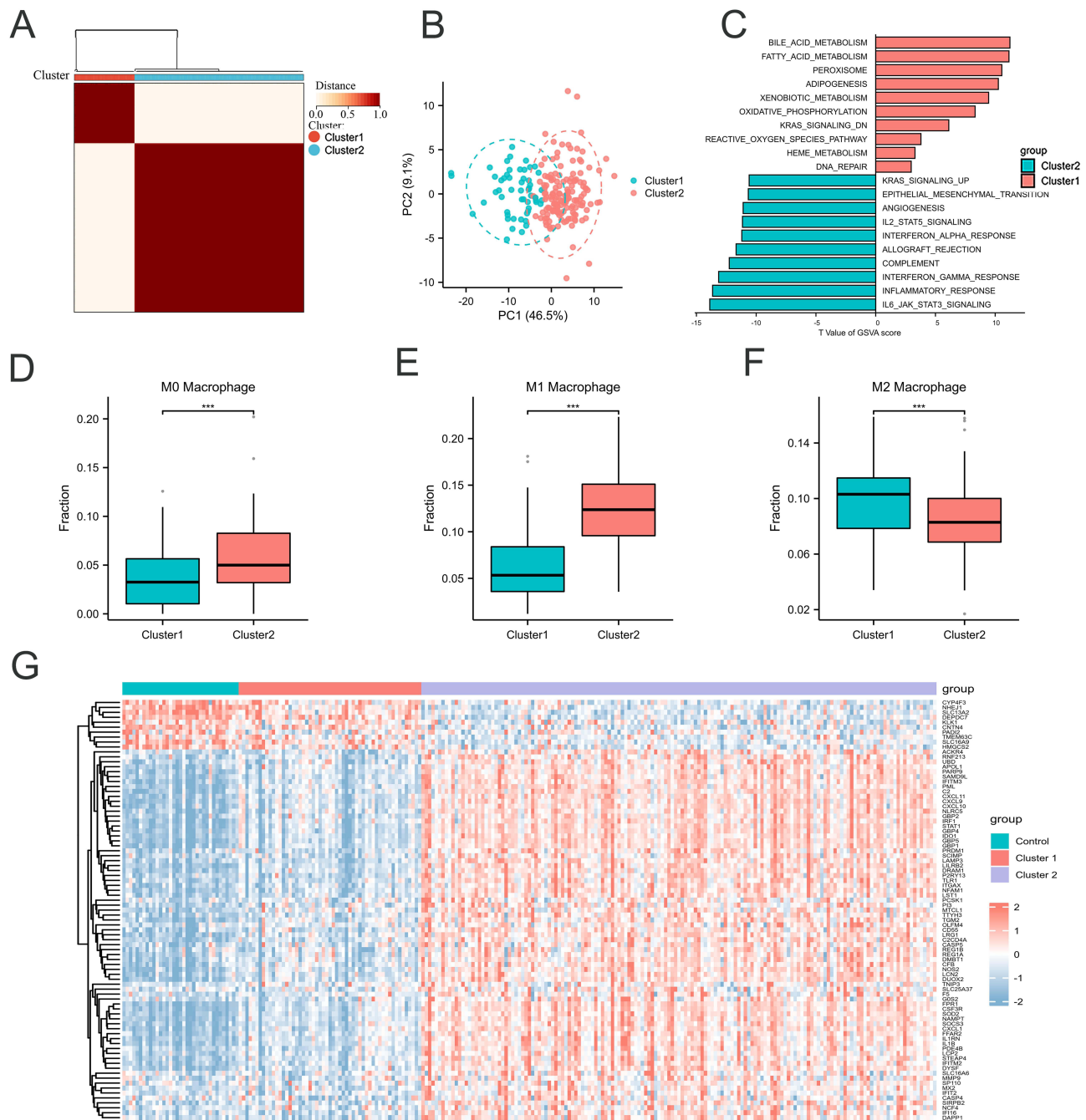
Figure 4 Identification of macrophage-related clusters in CD. (**A**) Consensus clustering matrices of MRGs (k = 2). (**B**) PCA of the expression of MRGs to distinguish two clusters. (**C**) The top 10 enriched KEGG pathways for each cluster. (**D–F**) The infiltration levels of M0, M1, and M2 macrophages in each cluster. (**G**) Heatmaps of MRGs in the control, cluster 1, and cluster 2 groups. (***p < 0.001).

cohorts. For example, Dai-IJMS performed better than MacroSig in GSE57945 but performed weakly in GSE93624 (0.813) and GSE126124 (0.764). These results demonstrated that MacroSig has superior stability and better extrapolation potential than the other tested methods.

Clinical Correlation Analysis

To investigate the impact of two genes, which constitute MacroSig, on clinical characteristics, we used the GSE193677 to analyze the expression levels of genes related to different disease activities and inflamed/uninflamed tissues. As shown in
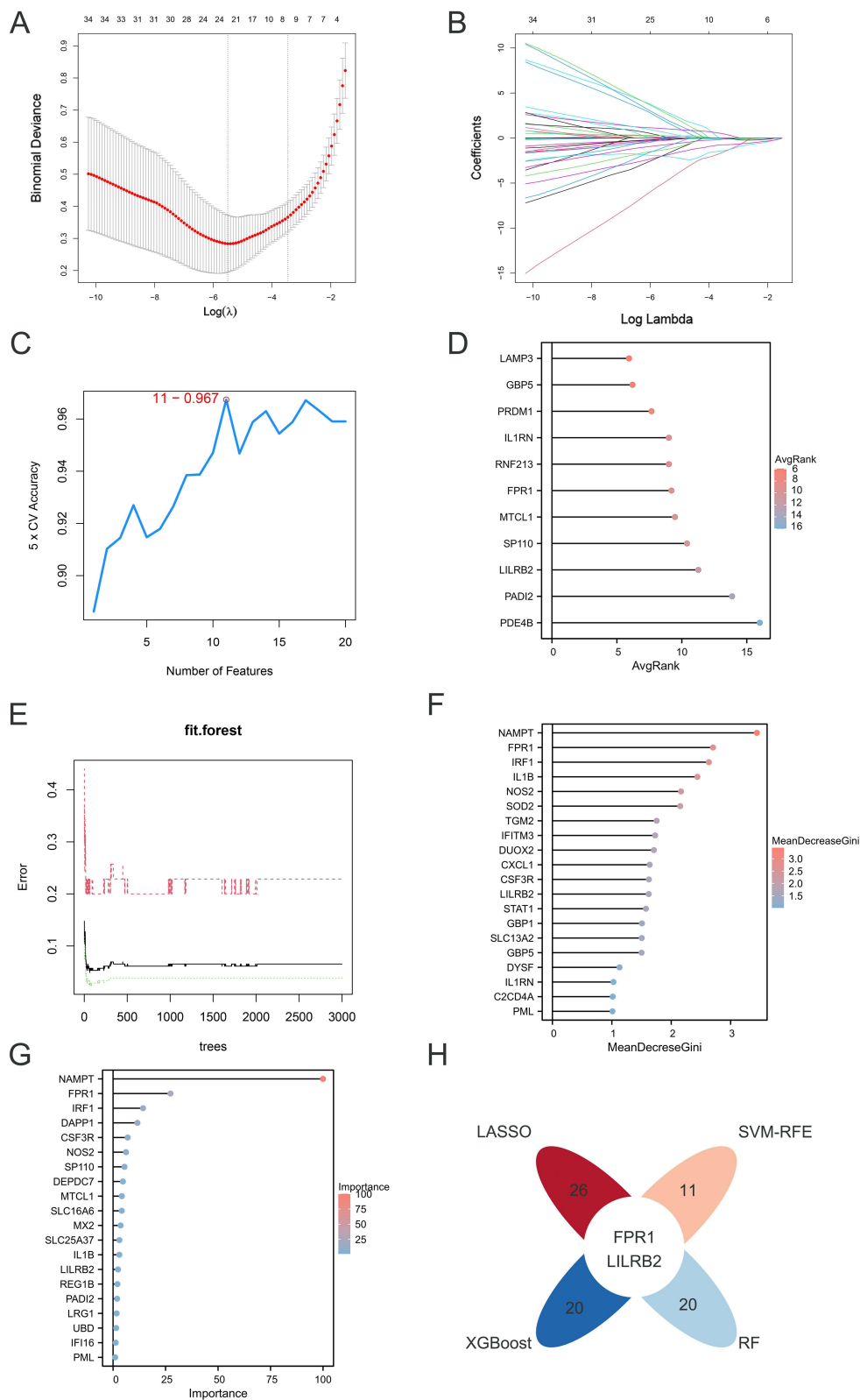
Figure 5 Screening potential biomarkers by machine learning (**A**) LASSO coefficient profiles. (**B**) Selection of the optimal tuning parameter (λ). (**C**) Estimating fivefold cross-validation accuracy using SVM-RFE. (**D**) Lollipop chart of genes selected by SVM-RFE. (**E**) The correlation plot between the number of RF trees and model error. (**F**) The top 20 genes selected by RF. (**G**) The top 20 genes selected by XGBoost. (**H**) Petal diagram of the intersection of the four machine learning algorithms.

Figure 6 Construction of MacroSig. (**A**) A total of 113 kinds of diagnostic models were evaluated via a 10-fold cross-validation framework, and AUC of each model was calculated across all the validation datasets. (**B–F**) AUC analysis of MacroSig and 6 published models in GSE93624, GSE57945, GSE179285, GSE16879, and GSE126124, respectively.

Figure 7A, the expression of FPR1 was higher in patients with active versus inactive disease, as defined by Harvey-Bradshaw index (HBI) scores, whereas the expression of LILRB2 was not different between the two groups. We observed a positive correlation between FPR1 expression and endoscopic assessments of severity according to the Simple Endoscopic Score for CD (SES-CD) (Figure 7B). FRP1 and LILRB2 were expressed at significantly higher levels in endoscopic-defined inflamed biopsies than those of non-inflamed and control biopsies (Figure 7C). Notably, the expression level of FPR1 was significantly higher in non-inflamed biopsies than in non-IBD control biopsies (Figure 7C). Overall, these data suggest that FPR1 is sensitive at detecting disease activity and can also distinguish disease from non-disease state.

Infliximab, a tumor necrosis factor inhibitor, was the first biological response modifier used to treat CD.[36,37] The effects of infliximab on FPR1 and LILRB2 were estimated using the GSE16879. The expression of FPR1 and LILRB2 was higher in nonresponders than in responders (Figure 7D). We further analyzed the ability of FPR1 and LILRB2 to distinguish responders from nonresponders. As shown in Figure 7E, FPR1 (AUC =0.891) had a better predictive ability to easily distinguish responders and non-responders before treatment than LILRB2 (AUC =0.847). For patients after treatment, FPR1 (AUC =0.991) also had better discriminatory ability for responders and nonresponders than LILRB2 (AUC =0.966) (Figure 7F).

Validation of the Expression of FPR1

Considering the strong correlation between FPR1 and clinical features and its higher importance in machine learning (Figure 7A–F and Figure 5D–G), we selected FPR1 for further analysis. In the training dataset GSE93624, the expression of FPR1 was significantly upregulated in tissues from patients with CD compared to those from the control group. FPR1 also exhibited outstanding diagnostic efficacy, with an AUC of 0.960 (Figure 8A). We further confirmed that FPR1 was highly expressed in both intestinal tissues (GSE57945, GSE179285, GSE6879, and GSE126124) and macrophages (GSE123141) from patients with CD compared to non-IBD controls. Notably, FPR1 demonstrated outstanding performance for CD diagnosis in all the validation datasets (Figure 8B–F). In addition, FPR1 expression was increased in cluster 2 (the high inflammatory level cluster), and FPR1 showed excellent performance in distinguishing between cluster
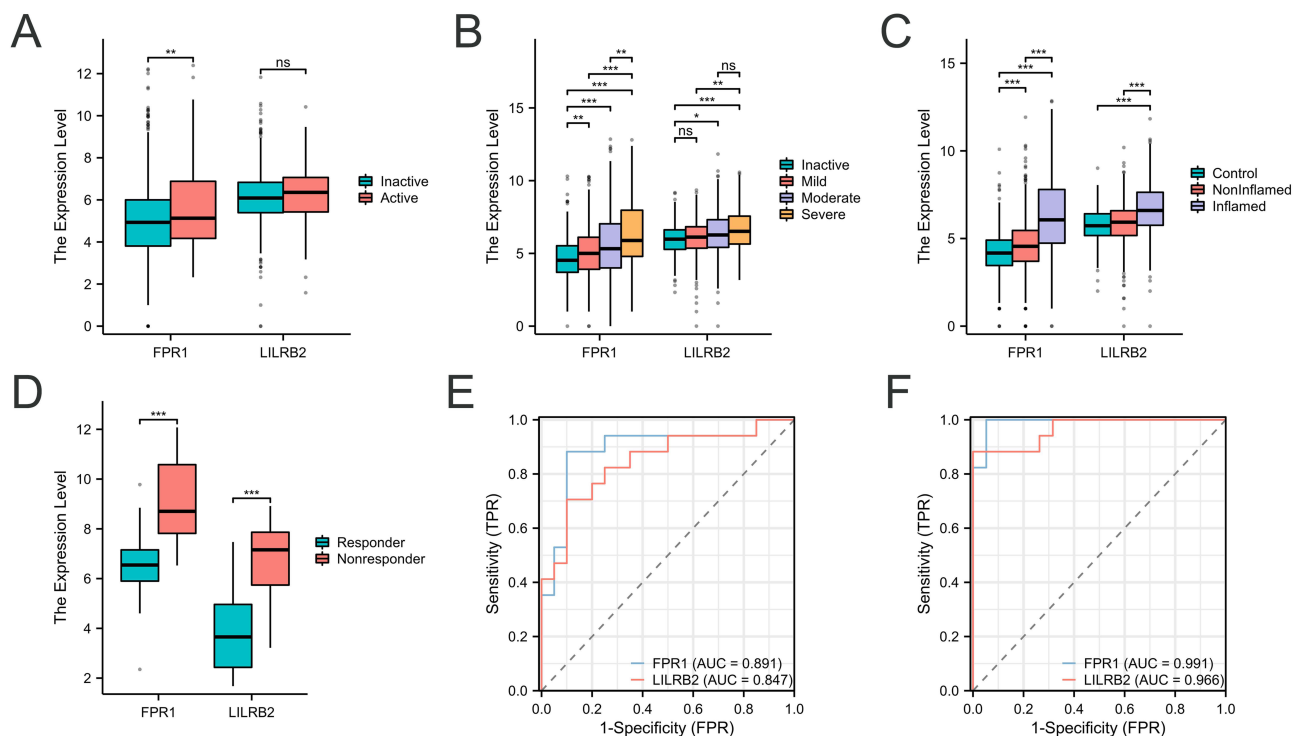
Figure 7 Clinical correlation analysis. The expression levels of FPR1 and LILRB2 in (**A**) Inactive and active groups defined by HBI. (**B**) Inactive, mild, moderate, and severe patients defined by SES-CD. (**C**) Control, Noninflamed, and inflamed biopsies. (**D**) Infliximab treatment responders and nonresponders. (**E** and **F**) ROC curves of FPR1 and LILRB2 for distinguishing responders and nonresponders before and after infliximab treatment in the GSE16879. (*p < 0.05, **p < 0.01, ***p < 0.001; ns, not significant).
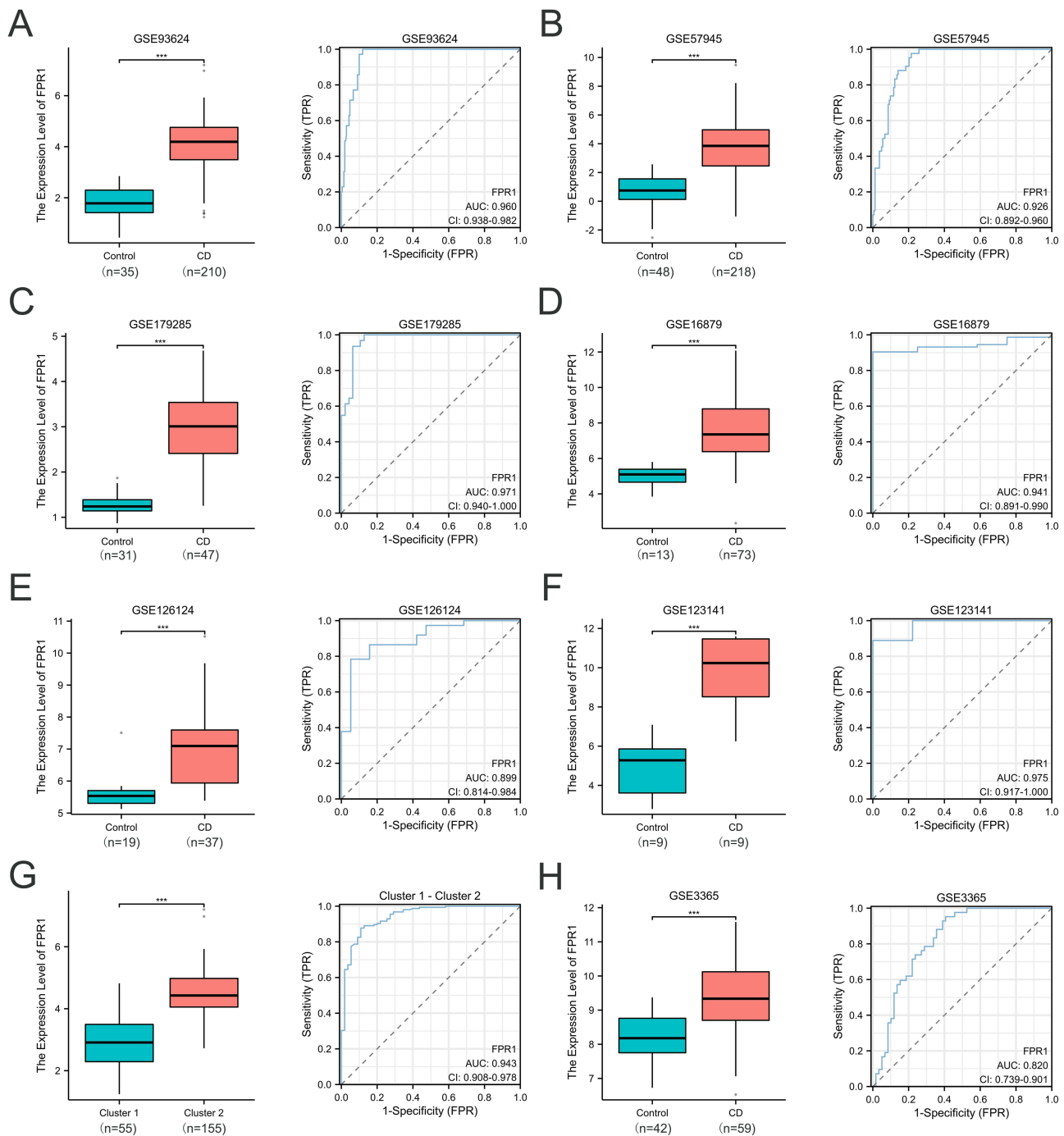
Figure 8 Diagnostic ability of FPR1. (**A–F** and **H**) The expression level and ROC curve of FPR1 for distinguishing control and CD in GSE93624, GSE57945, GSE179285, GSE16879, GSE126124, GSE123141, and GSE3365, respectively. (**G**) The expression level and ROC curve of FPR1 for distinguishing cluster 1 and cluster 2. (***p < 0.001).

2 and cluster 1 (Figure 8G). Considering that FPR1 was screened from macrophages isolated from the intestines of CD patients, and macrophages in the intestinal mucosa are continuously renewed by circulating monocytes.[38] We hypothesized that FPR1 in peripheral blood mononuclear cells (PBMCs) might be a diagnostic biomarker. In GSE3365, the expression of FPR1 was significantly upregulated in PBMCs isolated from CD patients compared to normal donors, whereas FPR1 showed efficient diagnostic performance in PBMCs, with an AUC of 0.820 (Figure 8H).

Subsequently, we collected FFPE tissue samples to validate the expression of FPR1 by IHC. Consistent with the results of previous bioinformatics analyses, FPR1 was highly expressed in CD tissues than in non-CD tissues (Figure 9A and B). To
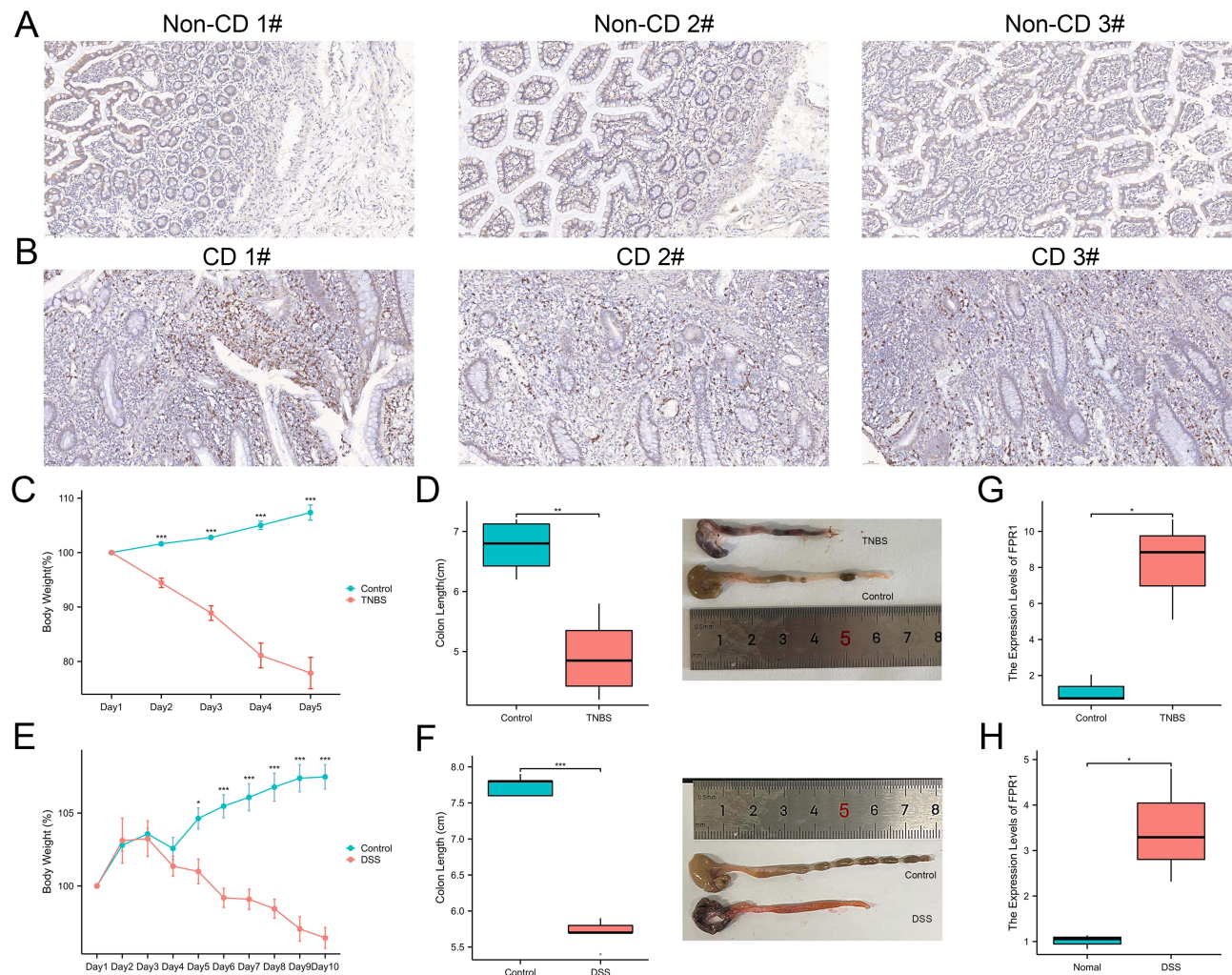
Figure 9 Validation of the FPR1 expression level (**A** and **B**) IHC staining of FPR1 in non-CD and CD tissues. (**C** and **D**) Body weight curves and colon length of TNBS-induced colitis mice. (**E** and **F**) Body weight curves and colon length of DSS-induced colitis mice. (**G** and **H**) The expression levels of FPR1 in TNBS- and DSS-induced colitis mice. (*$p < 0.05$, ***$p < 0.001$).

further verify our findings, DSS- and TNBS-induced colitis murine models were constructed by analyzing weight loss and colon length. Compared to those in the control groups, mice exposed to DSS or TNBS exhibited a decrease in body weight and a significant decrease in colon length (Figure 9C–F). Consistent with the findings in human CD, the expression of FPR1 was obviously increased in the colon tissues of both mice treated with DSS and those treated with TNBS (Figure 9G and H).

Role of FPR1 in Macrophage Polarization

We further analyzed scRNA-seq data from the Single Cell Portal to investigate the association between FPR1 and macrophages. tSNE analysis of FPR1 expression and cell types in CD patients demonstrated that FPR1 was major expressed in monocytes and macrophages (Figure 10A and B).

Given the strong association between FPR1 and macrophages, we utilized RAW264.7 cells and PMs to investigate the role of FPR1. Upregulation of FPR1 expression was observed in both M1-polarized RAW264.7 cells and PMs (Figure 10C and D). We further explored whether activating FPR1 could promote M1 macrophage polarization. To address this, we employed fMLP, a high-affinity ligand of FPR1, to activate FPR1 in RAW264.7 cells and PMs. The expression levels of cluster of differentiation 86 (CD86) and IL1β, markers of M1 polarization, were significantly increased after fMLP stimulation (Figure 10E–H). Furthermore, flow cytometry analysis revealed that proportion of CD86$^+$ cells was significantly increased after fMLP stimulation (Figure 10I and J). These findings demonstrated that
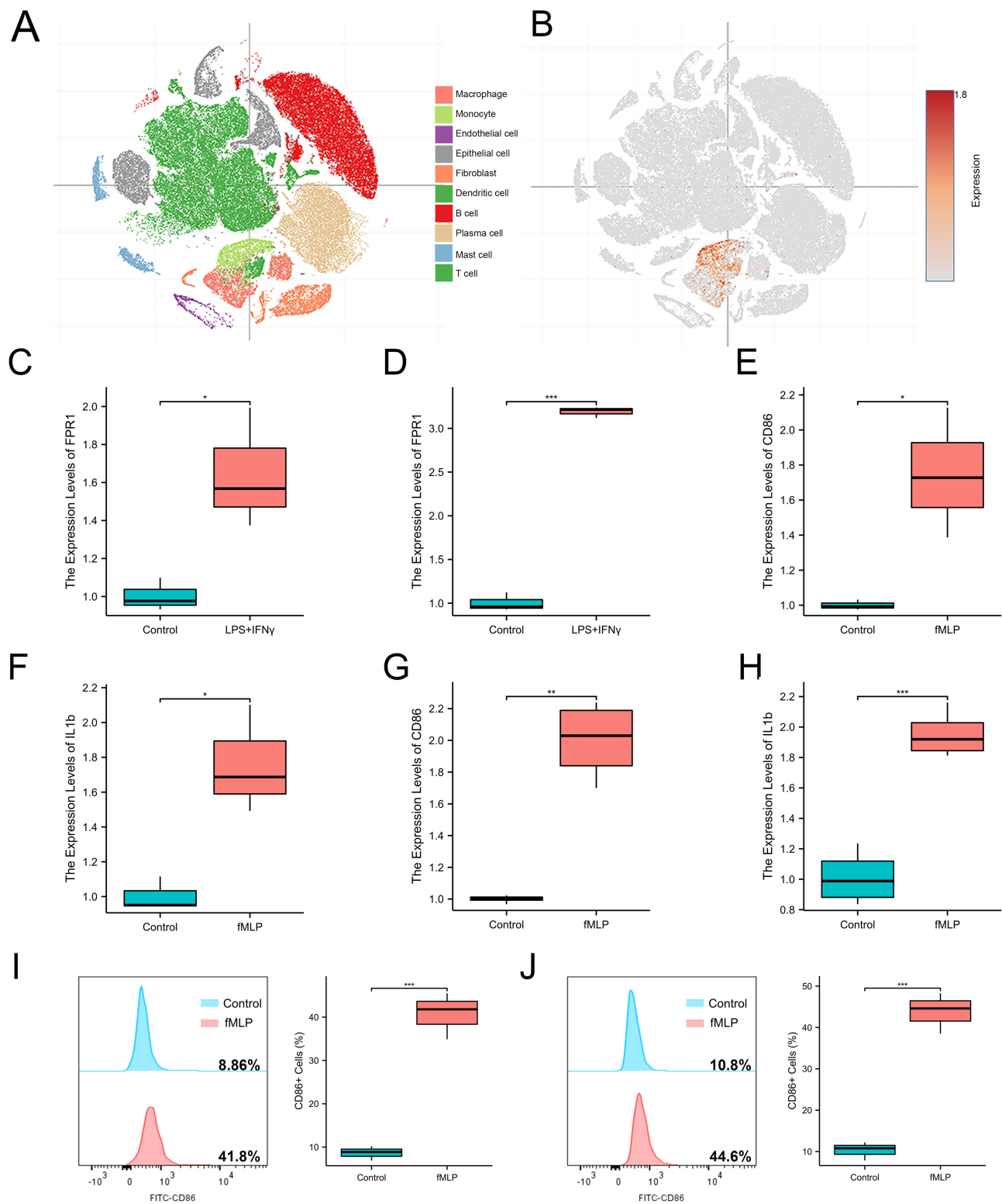
Figure 10 Role of FPR1 in macrophages. (**A** and **B**) tSNE map of cell types and FPR1 expression in the scRNA-seq data. (**C** and **D**) The expression levels of FPR1 in LPS-induced M1-polarized RAW264.7 cells and PMs. (**E** and **F**) The expression levels of CD86 and IL-1β in RAW264.7 cells after fMLP treatment. (**G** and **H**) The expression levels of CD86 and IL-1β in PMs after fMLP treatment, respectively.(**I** and **J**) Flow cytometry analysis of the expression of CD86 in RAW 264.7 and PMs, respectively. (*p < 0.05, **p < 0.01, ***p < 0.001).

FPR1 could promote M1 macrophage polarization. Overall, FPR1 is implicated in M1 polarization, and its activation promotes M1 polarization in macrophages.

Discussion

Macrophages play a vital role in maintaining homeostasis in the intestines.[8] Classically, the stepwise loss of balance in macrophage polarization initiates inflammation in this tissue, with the consequent tissue infiltration by M1 macrophages.[39,40] M1 macrophages recruit and activate of T cells, with further promote Th1 and Th17 immunity response, eventually exacerbate tissue damage.[7,41] In this study, the MacroSig was identified using advanced machine learning techniques, which holds promise for improving the diagnostic accuracy of CD. Our findings shed light on the molecular mechanisms of CD by identifying MRGs derived from the expression profiles of intestinal macrophages isolated from CD patients, with a particular emphasis on the role of FPR1. FPR1 was strongly associated with disease activity, inflammatory processes and macrophage polarization in CD, revealing the critical role of macrophages in disease pathogenesis, as highlighted in previous research.[7,42]

In our analysis, the unsupervised clustering of MRGs revealed two distinct clusters, each characterized by unique patterns of macrophage infiltration. Notably, Cluster 2 exhibited high M0 and M1 macrophage infiltration and significant enrichment of inflammation-related biological processes, including the IL6/JAK/STAT3 signaling pathway. These findings align with previous research on CD.[13,43] Patients in Cluster 2 exhibited high inflammatory levels.

Machine learning is extensively utilized in biology for selecting biomarkers, recognizing patterns, and constructing predictive models, thereby enhancing medical diagnosis accuracy.[44–47] Utilizing a suite of machine learning algorithms—LASSO, SVM-RFE, XGBoost, and RF—we screened MRGs to pinpoint FPR1 and LILRB2 as potential biomarkers. Subsequently, using the expression profiles of FPR1 and LILRB2, we developed an integrative method to construct MacroSig. Validation across four independent datasets indicated that the optimal model was achieved through the combination of LASSO and glmBoost. MacroSig exhibited high accuracy and exceptional performance across five datasets. Furthermore, in comparison with various previously reported biomarkers and signatures, it displayed improved stability and potential for extrapolation. These findings highlight the potential of MacroSig as a robust and reliable diagnostic tool for CD.

For the clinical assessment of CD, the HBI and SES-CD are pivotal tools.[48,49] Our study revealed that the expression level of FPR1 was significantly higher in patients with active CD, as defined by the HBI score, than in those with inactive disease. Furthermore, we observed a positive correlation between FPR1 expression and endoscopic assessments of severity according to the SES-CD. This correlation with both HBI and SES-CD suggested the potential of FPR1 as a sensitive marker for detecting disease activity and distinguishing between active and inactive disease states in CD. Additionally, a significantly higher expression level of FPR1 was detected in endoscopically defined inflamed biopsies than in noninflamed and control biopsies. These findings further emphasize its potential as a biomarker for inflammation in CD. These findings collectively highlight the clinical significance of FPR1 not only as a diagnostic marker but also as a sensitive indicator of disease severity and inflammation in CD. Moreover, the differential expression of FPR1 in response to infliximab treatment also indicates its potential role in predicting treatment response. Infliximab, a TNF-alpha inhibitor, is a cornerstone in the management of CD, and the ability to predict its efficacy is a significant step toward personalized medicine in this field.[36,37] The clinical significance of FPR1 in CD is further highlighted by its potential role in the pathophysiology of this disease. The involvement of FPR1 in immune cell recruitment and activation suggests that it could be a key player in the inflammatory cascade characteristic of CD.[50] This finding aligns with the growing body of evidence emphasizing the importance of targeted therapies for CD, which aim to modulate specific components of the immune response.[51]

Additionally, the validation of FPR1 expression in our study adds a crucial aspect to our discoveries. By confirming the increased levels of FPR1 expression in patients with CD through the examination of human tissue samples, we offer concrete evidence that supports its identification as a biomarker. These findings were further reinforced by the successful development of two colitis mouse models, facilitating us to validate the expression of FPR1 in an experimental setting. This comprehensive methodology is essential for enhancing the diagnostic value of FPR1 and emphasizing its potential as a target for therapeutic approaches. The validation of FPR1 expression in both human tissue and animal models establishes a strong basis for recognizing FPR1 as a significant factor in CD, creating opportunities for precise treatments that could regulate its expression or activity within the disease context.

FPR1, primarily expressed in myeloid cells such as neutrophils, monocytes, and macrophages, plays a pivotal role in the immune response.[52] Our single-cell analysis validated that in patients with CD, FPR1 is predominantly expressed on monocytes and macrophages. Although the function of FPR1 in neutrophils has been extensively studied,[53–55] its role in macrophages, particularly in the context of CD, has not been thoroughly explored. The compromised intestinal mucosal barrier function in CD results in heightened systemic exposure to LPS and fMLP derived from gut microbiota. In our investigation, we noted an increase in FPR1 expression in M1-polarized macrophages.[56,57] In our study, we observed an upregulation of FPR1 in M1-polarized macrophages. Intriguingly, the presence of fMLP promoted the expression of CD86 and IL-1β, leading to enhanced M1 polarization of macrophages. Our findings imply that FPR1 may impact macrophage polarization, contributing to the inflammatory environment characteristic of CD. Moreover, FPR1 has been implicated in exacerbating inflammation in murine experimental colitis. Furthermore, FPR1 has been implicated in exacerbating inflammation in murine experimental colitis.[58] This evidence further supports the role of FPR1 in promoting inflammatory responses in CD and underscores its potential as a target for therapeutic intervention. Elucidating the role of FPR1 in modulating macrophage behavior could unveil new insights into the underlying mechanisms of CD, potentially paving the way for innovative therapeutic strategies that target macrophage polarization.

However, our study has several limitations. The retrospective nature of the data analysis necessitates caution, and prospective studies are needed to validate these findings. Furthermore, the mechanistic roles of FPR1 in mediating macrophage polarization and in the pathogenesis of CD warrant further investigation.

Conclusion

In conclusion, our study established a promising and reliable diagnostic signature, MacroSig, based on a variety of bioinformatics and machine learning approaches. Moreover, FPR1, which is mainly expressed by macrophages, is strongly correlated with multiple clinical features in CD patients. Activation of FPR1 promotes M1 macrophage polarization. Therefore, targeting FPR1 to regulate macrophage polarization may be a new therapeutic strategy for CD.

Abbreviations

CD, Crohn's disease; MacroSig, Macrophage-related signatures; FPR1, Formyl peptide receptor 1; MRGs, Macrophage-related genes; GEO, Gene Expression Omnibus; IBD, Inflammatory bowel disease; LPS, Lipopolysaccharide; TNF-α, Tumor necrosis factor alpha; IL, Interleukin; scRNA-seq, Single cell RNA sequencing; WGCNA, Weighted correlation network analysis; DEG, Differentially expressed gene; LASSO, Least absolute shrinkage and selection operator; SVM-RFE, Support vector machine recursive feature elimination; XGBoost, eXtreme Gradient Boosting; RF, Random Forest; Enet, elastic network; LDA, Linear Discriminant Analysis; GBM, Gradient Boosting Machine; AUC, Area under the curve; GO, Gene Ontology; KEGG, Kyoto Encyclopedia of Genes and Genomes; GSVA, Gene set variation analysis; MSigDB, Molecular Signatures Database; DSS, Dextran sulfate sodium salt; TNBS, 2,4,6-trinitro-Benzenesulfonic acid; fMLP, N-Formyl-Met-Leu-Phe; FFPE, Formalin-fixed, paraffin-embedded; PCA, Principal component analysis; LILRB2, Leukocyte immunoglobulin like receptor b2; HBI, Harvey-Bradshaw index; SES-CD, Simple Endoscopic Score for Crohn's disease; PBMCs, Peripheral blood mononuclear cells; PMs, peritoneal macrophages; CD86, Cluster of differentiation 86.

Data Sharing Statement

The original contributions presented in the study are included in the article/Supplementary Files, further inquiries can be directed to the corresponding author.

Ethics Approval and Informed Consent

Collection of human FFPE sample was authorized by the Ethical Review Board of Renmin Hospital, Wuhan University (WDRY2021-KS066) and performed in accordance with the Declaration of Helsinki. Informed consent was obtained from all subjects involved in the study. All animal studies were approved by the laboratory animal ethics committee of Renmin Hospital of Wuhan University [No. WDRM-20230702A]. All animal experiments were conducted following the Guide for the Care and Use of Laboratory Animals.[59]

Funding

Disclosure

The authors report no conflicts of interest in this work.

References

1. Torres J, Mehandru S, Colombel JF, Peyrin-Biroulet L. Crohn's disease. *Lancet*. 2017;389(10080):1741–1755. doi:10.1016/S0140-6736(16)31711-1
2. Baumgart DC, Sandborn WJ. Crohn's disease. *Lancet*. 2012;380(9853):1590–1605. doi:10.1016/S0140-6736(12)60026-9
3. Roda G, Chien Ng S, Kotze PG, et al. Crohn's disease. *Nat Rev Dis Primers*. 2020;6(1):22. doi:10.1038/s41572-020-0156-2
4. Ng SC, Tang W, Ching JY, et al. Incidence and phenotype of inflammatory bowel disease based on results from the Asia-pacific Crohn's and colitis epidemiology study. *Gastroenterology*. 2013;145(1):158–165 e152. doi:10.1053/j.gastro.2013.04.007
5. Bernstein CN. Treatment of IBD: where we are and where we are going. *Am J Gastroenterol*. 2015;110(1):114–126. doi:10.1038/ajg.2014.357
6. Kong L, Pokatayev V, Lefkovith A, et al. The landscape of immune dysregulation in Crohn's disease revealed through single-cell transcriptomic profiling in the ileum and colon. *Immunity*. 2023;56(2):444–458 e445. doi:10.1016/j.immuni.2023.01.002
7. Na YR, Stakenborg M, Seok SH, Matteoli G. Macrophages in intestinal inflammation and resolution: a potential therapeutic target in IBD. *Nat Rev Gastroenterol Hepatol*. 2019;16(9):531–543. doi:10.1038/s41575-019-0172-4
8. Hegarty LM, Jones GR, Bain CC. Macrophages in intestinal homeostasis and inflammatory bowel disease. *Nat Rev Gastroenterol Hepatol*. 2023;20 (8):538–553. doi:10.1038/s41575-023-00769-0
9. Atri C, Guerfali FZ, Laouini D. Role of human macrophage polarization in inflammation during infectious diseases. *Int J Mol Sci*. 2018;19(6):1801. doi:10.3390/ijms19061801
10. Murray PJ. Macrophage Polarization. *Annu Rev Physiol*. 2017;79(1):541–566. doi:10.1146/annurev-physiol-022516-034339
11. Liu X, Ren X, Zhou L, et al. Tollip orchestrates macrophage polarization to alleviate intestinal mucosal inflammation. *J Crohn's Colitis*. 2022;16 (7):1151–1167. doi:10.1093/ecco-jcc/jjac019
12. Mosser DM, Hamidzadeh K, Goncalves R. Macrophages and the maintenance of homeostasis. *Cell Mol Immunol*. 2021;18(3):579–587. doi:10.1038/s41423-020-00541-3
13. Cheng Y, Li J, Wang L, et al. Eriocalyxin B ameliorated Crohn's disease-like colitis by restricting M1 macrophage polarization through JAK2/ STAT1 signalling. *Eur J Pharmacol*. 2023;954:175876. doi:10.1016/j.ejphar.2023.175876
14. Ritchie ME, Phipson B, Wu D, et al. limma powers differential expression analyses for RNA-sequencing and microarray studies. *Nucleic Acids Res*. 2015;43(7):e47. doi:10.1093/nar/gkv007
15. Shen W, Song Z, Zhong X, et al. Sangerbox: a comprehensive, interaction-friendly clinical bioinformatics analysis platform. *Imeta*. 2022;1(3):e36. doi:10.1002/imt2.36
16. Langfelder P, Horvath S. WGCNA: an R package for weighted correlation network analysis. *BMC Bioinf*. 2008;9:559. doi:10.1186/1471-2105-9-559
17. Newman AM, Liu CL, Green MR, et al. Robust enumeration of cell subsets from tissue expression profiles. *Nat Methods*. 2015;12(5):453–457. doi:10.1038/nmeth.3337
18. Friedman J, Hastie T, Tibshirani R. Regularization paths for generalized linear models via coordinate descent. *J Stat Softw*. 2010;33(1):1–22. doi:10.18637/jss.v033.i01
19. Sanz H, Valim C, Vegas E, Oller JM, Reverter F. SVM-RFE: selection and visualization of the most relevant features through non-linear kernels. *BMC Bioinf*. 2018;19(1):432. doi:10.1186/s12859-018-2451-4
20. Chen T, Guestrin C XGBoost: a scalable tree boosting system. Proceedings of the 22nd ACM SIGKDD International Conference on Knowledge Discovery and Data Mining; San Francisco, California, USA; 2016.
21. Chen X, Ishwaran H. Random forests for genomic data analysis. *Genomics*. 2012;99(6):323–329. doi:10.1016/j.ygeno.2012.04.003
22. Liu Z, Liu L, Weng S, et al. Machine learning-based integration develops an immune-derived lncRNA signature for improving outcomes in colorectal cancer. *Nat Commun*. 2022;13(1):816. doi:10.1038/s41467-022-28421-6
23. Yu G, Wang LG, Han Y, He QY. clusterProfiler: an R package for comparing biological themes among gene clusters. *OMICS*. 2012;16(5):284–287. doi:10.1089/omi.2011.0118
24. Walter W, Sanchez-Cabo F, Ricote M. GOplot: an R package for visually combining expression data with functional analysis. *Bioinformatics*. 2015;31(17):2912–2914. doi:10.1093/bioinformatics/btv300
25. Hanzelmann S, Castelo R, Guinney J. GSVA: gene set variation analysis for microarray and RNA-seq data. *BMC Bioinf*. 2013;14(1):7. doi:10.1186/ 1471-2105-14-7
26. Ye C, Zhu S, Yuan J. Construction of ceRNA network to reveal potential biomarkers in Crohn's disease and validation in a TNBS induced mice model. *J Inflamm Res*. 2021;14:6447–6459. doi:10.2147/JIR.S338053
27. Zhang X, Goncalves R, Mosser DM. The isolation and characterization of murine macrophages. *Curr Protoc Immunol*. 2008;14:14 11 11–14 11 14.
28. Kammerer U, Kapp M, Gassel AM, et al. A new rapid immunohistochemical staining technique using the EnVision antibody complex. *J Histochem Cytochem*. 2001;49(5):623–630. doi:10.1177/002215540104900509
29. Vamathevan J, Clark D, Czodrowski P, et al. Applications of machine learning in drug discovery and development. *Nat Rev Drug Discov*. 2019;18 (6):463–477. doi:10.1038/s41573-019-0024-5
30. Wu H, Zeng R, Qiu X, et al. Investigating regulatory patterns of NLRP3 Inflammasome features and association with immune microenvironment in Crohn's disease. *Front Immunol*. 2022;13:1096587. doi:10.3389/fimmu.2022.1096587
31. Dai Z, Zhang J, Xu W, Du P, Wang Z, Liu Y. Single-cell sequencing-based validation of T cell-associated diagnostic model genes and drug response in Crohn's disease. *Int J Mol Sci*. 2023;24(7):6054. doi:10.3390/ijms24076054
32. Chen X, Gao Y, Xie J, et al. Identification of FCN1 as a novel macrophage infiltration-associated biomarker for diagnosis of pediatric inflammatory bowel diseases. *J Transl Med*. 2023;21(1):203. doi:10.1186/s12967-023-04038-1

33. Zhang X, Chen T, Qian X, He X, V E S. Bioinformatics analysis of immune cell infiltration and diagnostic biomarkers between ankylosing spondylitis and inflammatory bowel disease. *Comput Math Methods Med*. 2023;2023:9065561. doi:10.1155/2023/9065561

34. Ye C, Huang Y, Gao Y, Zhu S, Yuan J. Exploring the glycolytic cross-talk genes between inflammatory bowel disease and colorectal cancer. *Funct Integr Genomics*. 2023;23(3):230. doi:10.1007/s10142-023-01170-5

35. Huang R, Wang W, Chen Z, et al. Identifying immune cell infiltration and effective diagnostic biomarkers in Crohn's disease by bioinformatics analysis. *Front Immunol*. 2023;14:1162473. doi:10.3389/fimmu.2023.1162473

36. Adegbola SO, Sahnan K, Warusavitarne J, Hart A, Tozer P. Anti-TNF Therapy in Crohn's Disease. *Int J Mol Sci*. 2018;19(8):2244. doi:10.3390/ijms19082244

37. Ye C, Zhu S, Yuan J. Characterization of two TNF-related subtypes predicting infliximab therapy responses in Crohn's disease. *Front Immunol*. 2022;13:871312. doi:10.3389/fimmu.2022.871312

38. Ginhoux F, Jung S. Monocytes and macrophages: developmental pathways and tissue homeostasis. *Nat Rev Immunol*. 2014;14(6):392–404. doi:10.1038/nri3671

39. Wang K, Mao T, Lu X, et al. A potential therapeutic approach for ulcerative colitis: targeted regulation of macrophage polarization through phytochemicals. *Front Immunol*. 2023;14:1155077. doi:10.3389/fimmu.2023.1155077

40. Zhang K, Guo J, Yan W, Xu L. Macrophage polarization in inflammatory bowel disease. *Cell Commun Signal*. 2023;21(1):367. doi:10.1186/s12964-023-01386-9

41. Dharmasiri S, Garrido-Martin EM, Harris RJ, et al. Human intestinal macrophages are involved in the pathology of both ulcerative colitis and Crohn disease. *Inflamm Bowel Dis*. 2021;27(10):1641–1652. doi:10.1093/ibd/izab029

42. Yang S, Zhao M, Jia S. Macrophage: key player in the pathogenesis of autoimmune diseases. *Front Immunol*. 2023;14:1080310. doi:10.3389/fimmu.2023.1080310

43. Jin L, Li L, Hu C, et al. Integrative analysis of transcriptomic and proteomic profiling in inflammatory bowel disease colon biopsies. *Inflamm Bowel Dis*. 2019;25(12):1906–1918. doi:10.1093/ibd/izz111

44. Greener JG, Kandathil SM, Moffat L, Jones DT. A guide to machine learning for biologists. *Nat Rev Mol Cell Biol*. 2022;23(1):40–55. doi:10.1038/s41580-021-00407-0

45. Richens JG, Lee CM, Johri S. Improving the accuracy of medical diagnosis with causal machine learning. *Nat Commun*. 2020;11(1):3923. doi:10.1038/s41467-020-17419-7

46. Mahendran N, Durai Raj Vincent PM, Srinivasan K, Chang CY. Machine learning based computational gene selection models: a survey, performance evaluation, open issues, and future research directions. *Front Genet*. 2020;11:603808. doi:10.3389/fgene.2020.603808

47. He X, Ye H, Zhao R, et al. Advanced machine learning model for predicting Crohn's disease with enhanced ant colony optimization. *Comput Biol Med*. 2023;163:107216. doi:10.1016/j.compbiomed.2023.107216

48. Daperno M, D'Haens G, Van Assche G, et al. Development and validation of a new, simplified endoscopic activity score for Crohn's disease: the SES-CD. *Gastrointest Endosc*. 2004;60(4):505–512. doi:10.1016/S0016-5107(04)01878-4

49. Best WR. Predicting the Crohn's disease activity index from the Harvey-Bradshaw index. *Inflamm Bowel Dis*. 2006;12(4):304–310. doi:10.1097/01.MIB.0000215091.77492.2a

50. Chen K, Bao Z, Gong W, Tang P, Yoshimura T, Wang JM. Regulation of inflammation by members of the formyl-peptide receptor family. *J Autoimmun*. 2017;85:64–77. doi:10.1016/j.jaut.2017.06.012

51. Neurath MF. Cytokines in inflammatory bowel disease. *Nat Rev Immunol*. 2014;14(5):329–342. doi:10.1038/nri3661

52. Jeong YS, Bae YS. Formyl peptide receptors in the mucosal immune system. *Exp Mol Med*. 2020;52(10):1694–1704. doi:10.1038/s12276-020-00518-2

53. Dorward DA, Lucas CD, Chapman GB, Haslett C, Dhaliwal K, Rossi AG. The role of formylated peptides and formyl peptide receptor 1 in governing neutrophil function during acute inflammation. *Am J Pathol*. 2015;185(5):1172–1184. doi:10.1016/j.ajpath.2015.01.020

54. Li Z, Li Y, Han J, et al. Formyl peptide receptor 1 signaling potentiates inflammatory brain injury. *Sci Transl Med*. 2021;13(605). doi:10.1126/scitranslmed.abe9890

55. Kuley R, Stultz RD, Duvvuri B, et al. N-formyl methionine peptide-mediated neutrophil activation in systemic sclerosis. *Front Immunol*. 2021;12:785275. doi:10.3389/fimmu.2021.785275

56. Pasternak BA, D'Mello S, Jurickova II, et al. Lipopolysaccharide exposure is linked to activation of the acute phase response and growth failure in pediatric Crohn's disease and murine colitis. *Inflamm Bowel Dis*. 2010;16(5):856–869. doi:10.1002/ibd.21132

57. Wollam J, Riopel M, Xu YJ, et al. Microbiota-produced N-formyl peptide fMLF promotes obesity-induced glucose intolerance. *Diabetes*. 2019;68(7):1415–1426. doi:10.2337/db18-1307

58. Di Paola R, Fusco R, Gugliandolo E, et al. Formyl peptide receptor 1 signalling promotes experimental colitis in mice. *Pharmacol Res*. 2019;141:591–601. doi:10.1016/j.phrs.2019.01.041

59. The National Academic press. *Guide for the Care and Use of Laboratory Animals*. 8th ed. Washington (DC): The National Academic press; 2011.